BOULDER DISTRIBUTIONS AT LEGACY LANDING SITES: ASSESSING REGOLITH PRODUCTION RATES AND LANDING SITE HAZARDS. R. N. Watkins[1,2], B. L. Jolliff[1], S. J. Lawrence[3], P.O. Hayne[4], R. R. Ghent[2,5], [1]Washington University in St. Louis and the McDonnell Center for the Space Sciences, Campus Box 1169, 1 Brookings Dr., Saint Louis, MO 63130, rclegg@levee.wustl.edu, [2]Planetary Science Institute, Tucson, AZ, [3]NASA Johnson Space Center, Houston, TX, [4]NASA-Jet Propulsion Laboratory, Pasadena, CA, [5]Dept. of Earth Sciences, University of Toronto, Toronto, ON, Canada.

Introduction: Understanding how the distribution of boulders on the lunar surface changes over time is key to understanding small-scale erosion processes and the rate at which rocks become regolith. Boulders degrade over time, primarily as a result of micrometeorite bombardment [1,2], so their residence time at the surface can inform the rate at which rocks become regolith or become buried within regolith. Because of the gradual degradation of exposed boulders, we expect that the boulder population around an impact crater will decrease as crater age increases. Boulder distributions around craters of varying ages are needed to understand regolith production rates, and Lunar Reconnaissance Orbiter Camera (LROC) Narrow Angle Camera (NAC) images [3] provide one of the best tools for conducting these studies. Using NAC images to assess how the distribution of boulders varies as a function of crater age provides key constraints for boulder erosion processes.

Boulders also represent a potential hazard that must be addressed in the planning of future lunar landings. A boulder under a landing leg can contribute to deck tilt, and boulders can damage spacecraft during landing. Using orbital data to characterize boulder populations at locations where landers have safely touched down (Apollo, Luna, Surveyor, Chang'e-3) provides validation for landed mission hazard avoidance planning. Additionally, counting boulders at legacy landing sites is useful because: 1) LROC has extensive coverage of these sites at high resolutions (~0.5 m/pixel). 2) Returned samples from craters at these sites have been radiometrically dated, allowing assessment of how boulder distributions vary as a function of crater age. 3) Surface photos at these sites can be used to correlate with remote sensing measurements.

Most boulder populations occur in association with steep slopes as a result of mass wasting or around young, fresh craters that are large enough to have excavated bedrock [4-7]. Here we use NAC images to analyze boulder distributions around three craters of varying sizes and ages: Cone crater (CC; 26 Ma [8], 340 m diameter) at the Apollo 14 site (**Fig. 1**), North Ray crater (NR; 50 Ma [8], 950 m) at Apollo 16, and Surveyor Crater (SC; 200 Ma [8], 200 m) at Apollo 12.

Methods: We use CraterTools [9] in ArcMap to visually identify and estimate the size of boulders. In NAC images, boulders are positive relief features and appear as bright, sun-facing pixels adjacent to dark, generally elongated shadows in low-sun images. Boulder sizes are recorded in terms of a circular diameter to capture the longest dimension. Using NAC images with a 0.5 m/pixel resolution, the smallest boulders that can be identified with confidence are ~1 m (>3 pixels including the shadow). We determine the distance of each boulder from the center of the crater using the haversine formula.

Boulder Distributions: The distributions we investigate are boulder size-range distributions, size-frequency distributions, and frequency-range distributions. These distributions are important for understanding how far craters of varying sizes and ages distribute boulders. We determine boulder distributions at increasing distances (in units of crater radii) to find how the frequency of boulders varies as a function of dis-

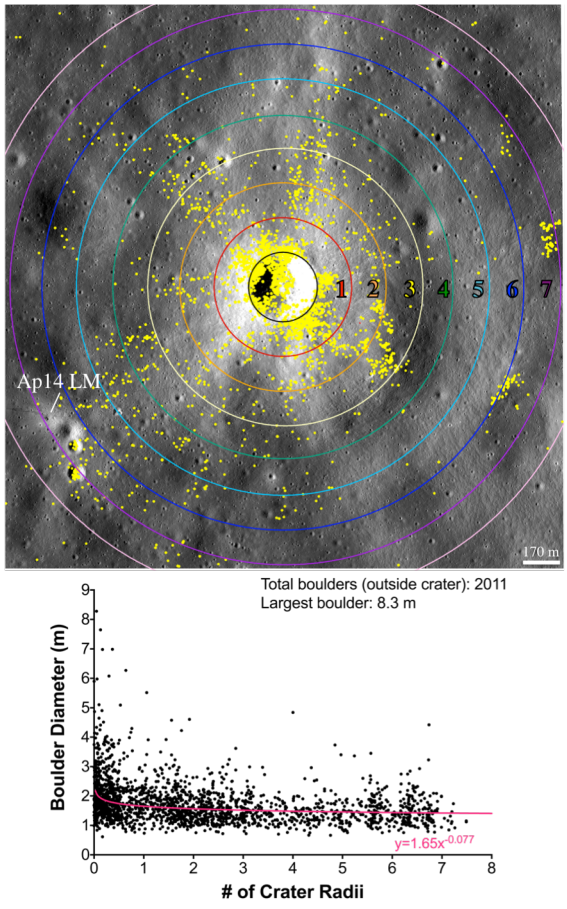

Fig. 1: Top: Boulder counts centered at Cone crater. Colored circles and numbers indicate distances from the rim (black circle) in crater radii. Bottom: Size-range distribution of boulders around Cone. Larger boulders lie closer to the rim and few boulders are seen beyond 8 crater radii.

tance from the crater rim. We omit boulders inside the rim, because steep slopes inside rims tend to refresh the rock population as crater degradation proceeds.

Results: Our boulder distributions show that the largest boulders within a count area occur closer to the crater rim (within ~2-4 crater radii) and smaller boulders occur at all distances (**Fig. 1**). The largest boulders seen are ~8 m at Cone, ~22 m at North Ray, and ~4 m at Surveyor. The quantity (areal density) of boulders decreases with increasing distance from the crater rim. The presence of boulders drops off around 8 crater radii for both CC and NR. Fewer boulders are seen around SC, and the size- and range-frequency distributions are irregular compared to NR and CC.

Implications: Because boulders degrade over time, in principle, more boulders should be present around younger craters. Previous studies have shown a strong relationship between crater age and ejecta rockiness [10,11], with m-scale boulder survival rates at craters <1 km in diameter on the order of ~150-300 Ma [10]. Our counts agree with this conclusion so far; fewer boulders are present at the older Surveyor crater (200 Ma) than at the younger CC and NR craters. CC and NR are young relative to the estimated time required to break down boulders [10,11], so most of their boulders are still present on the surface. Cumulative rock abundances around craters of varying ages will help constrain the boulder survival rates more accurately.

Size is also important – larger craters tend to excavate more boulders than smaller craters, and the size of the largest boulder ejected is likely related to the size of the crater [12-15]. We see both a higher number and larger boulders present around the larger NR crater than around CC and SC. Power-law fits to the size-range and -frequency distributions, of the form $y=ax^{-b}$, for craters of varying size will provide enough a and b values to allow us to derive equations to predict these values as a function of crater size. These derived equations can then be used to estimate the maximum boulder size expected at a crater of a given size.

The presence of fewer boulders and the irregular frequency distributions at SC are likely owing to its location in the vicinity of several other fresh craters with their own boulder distributions, as well as to its smaller size and older age. The boulders that are present around SC are much smaller than those seen at the two younger craters, owing to its smaller diameter. Counts at more craters with varying sizes and ages (and far from other fresh craters) will allow us to better constrain boulder survival rates and test quantitative models set forth by previous studies [*i.e.*, 11].

Surface Photography: The location and size of boulders imaged and sampled by Apollo astronauts are very well documented, enabling comparison with and verification of our NAC measurements. We have used Apollo 14 and Apollo 16 surface photographs and boulder measurements [16,17] to locate and validate size measurements of boulders.

Diviner Rock Abundance: NAC boulder distributions can also be used to validate Diviner rock abundance (DRA) data, which measures the areal density of the surface covered in boulders [4]. We calculate the cumulative areal fraction (CAF) of the surface covered in boulders at Cone and North Ray to compare with the RA values presented in [4], and find that our LROC counts closely predict the same CAF as DRA values.

Landing Site Safety: Finally, the results from boulder counts on ejecta blankets will provide constraints on how far craters of varying sizes distribute boulders. Predicting boulder size distributions as a function of distance from a crater is particularly useful in informing potential boulder hazards for future missions. Boulder distributions can be used to estimate and automate counts for future missions using the power-law relationships derived from size-range distributions. Coupling LROC data with DRA also allows us to extrapolate boulder count trends to sub-meter boulder populations that are unresolvable with NAC images and that may also pose a landing hazard [18].

Future Work: Ongoing work includes conducting more counts of boulder populations around craters of varying ages and testing key parameters such as crater size, degradation state, terrain type (mare vs. nonmare), and regolith thickness on boulder populations. This work will allow us to more comprehensively assess how boulder distributions change as a function of time, thereby informing the median survival time of boulders and the Moon's regolith production rates. When coupled with counts at other spacecraft landing sites and verified using surface photography, these results can also inform boulder populations at varying distances from craters and aid in establishing safe landing zones for future missions [13,14].

Acknowledgements: We thank the LROC Operations Team for image collection and processing, and we thank NASA for support of the LRO mission.

References: [1] Gault et al. (1972) *LSC III*, 2713-2744 [2] Hörz, et al. (1975) *Moon, 13,* 235-258. [3] Robinson et al. (2010) *Space Sci. Rev. 150,* 81–124. [4] Bandfield et al. (2011) *JGR 116.* [5] Lawrence et al. (2013) *JGR 118,* 615–634. [6] Jawin et al. (2014) *JGR-P., 119,* 2331–2348. [7] Shoemaker (1965) *JPL Tech. Report #32-700*, 76-134. [8] Arvidson et al. (1975) *Moon, 13*, 259–276. [9] Kneissl et al. (2011) *PSS, 59,* 1243–1254. [10] Basilevsky et al. (2013), *PSS, 89,* 118–126. [11] Ghent et al. (2014) *Geology, 42,* 1059–1062. [12] Moore (1971) *NASA SP-232*, 26-27. [13] Cintala and McBride (1995) *NASA TM-104804.* [14] Bart and Melosh (2010) *Icarus, 209,* 337–357. [15] Krishna and Kumar (2016) *Icarus, 264,* 274-299. [16] Swann et al. (1977) *Geo. Surv. Prof. Paper 880.* [17] Ulrich (1981) *Geo. Surv. Prof. Paper 1048.* [18] Elder et al. (2016) *AGU Fall Mtg,* Abstract #P24A-04.